Electron Transfer Reactions of Anthracene Adsorbed on Silica Gel

David R. Worrall, Siân L. Williams, and Francis Wilkinson*

Department of Chemistry, Loughborough University, Loughborough, Leicestershire LE11 3TU, U.K.

Received: January 8, 1997; In Final Form: April 8, 1997[⊗]

The production and decay of the anthracene radical cation on silica gel has been studied using nanosecond time-resolved diffuse reflectance laser flash photolysis. The production of the radical cation has been shown to be via a multiphoton process both by a laser dose study and by millisecond flashlamp experiments. The decay kinetics of the radical cation conform well to an analysis based on geminate recombination at loadings of less than 2 μmol g^{-1}. At higher loadings, deviations from these kinetics are observed caused by bulk electron diffusion competing efficiently with geminate recombination. Addition of electron donors such as triphenylamine, *N*,*N*,*N*′,*N*′-tetramethyl-1,4-phenylenediamine, *N*,*N*-dimethylaniline, and azulene greatly accelerate the rate of radical ion decay via an electron transfer mechanism. Kinetic analysis reveals that the observed decay can be described by either the dispersive kinetic model of Albery et al. or a fractal dimensional rate constant model of the type which has been used to describe triplet−triplet annihilation on surfaces. The bimolecular rate constants vary considerably and do not show a simple dependence on the free energy for electron transfer. This can be explained either on the basis of bulk diffusion of electron donors being slow relative to the electron transfer process, or by the presence of a Marcus "inverted region" at relatively modest negative free energy values.

Introduction

The photophysical and photochemical behavior of adsorbates on solid substrates can provide valuable information regarding the interactions between the adsorbate and the substrate, the nature of the adsorption sites, and the mobility restrictions imposed on the probe by the surface. The mobility of molecules on surfaces has been probed by studies of triplet−triplet annihilation[1−3] and dynamic excimer formation[4] following laser excitation of a single adsorbed species. Other methods for studying diffusion on surfaces have involved the coadsorption of different molecular species which undergo energy[5,6] or electron[6] transfer. These studies have shown that many molecules diffuse rapidly on the surfaces of silica gel and γ-alumina and that the mobility of the adsorbed molecules is greatly influenced by the temperature to which the substrate is heated to prior to adsorption.

The detection of aromatic radical cations through photoionization on silica gel,[3,7−10] γ-alumina,[5,6,11−14] and in zeolites[8,15−25] has previously been reported. The mechanism of production of the radical cation is dependent on the nature of the interactions between the molecule and the surface on which it is adsorbed. The ionization potentials of arenes are between 7 and 8 eV in the gas phase,[26] so photoionization following absorption of laser light of, for example, 355 nm (3.5 eV) would be expected to require two or more photons. Diffuse reflectance laser flash photolysis studies by us[3] and others have shown that bi- and multiphotonic production of aromatic radical cation tends to occur on silica gel[3,7] and γ-alumina[6,7,11] surfaces.

The decay of radical cations on oxide surfaces is generally via electron−radical cation recombination, regenerating the ground state. Oelkrug et al.[7] demonstrated this behavior using distyrylbenzenes adsorbed on silica gel and γ-alumina by repetitive excitation of the same sample area at room temperature. The observed transient absorption intensity and decay kinetics were insensitive to the degree of irradiation of the sample. The observed radical cation decay is usually complex, showing initially a very fast decay followed by slower components. Diphenylpolyenes[27] adsorbed on γ-alumina and distyrylbenzenes[7] adsorbed on silica gel and γ-alumina have been shown to decay by geminate recombination at very low loadings (between 7×10^{-7} and 3×10^{-9} mol g^{-1}). The decay profile of the pyrene radical cation adsorbed on γ-alumina[6] has been fitted with the dispersive kinetic model of Albery et al.[28] This model has also successfully been applied to describe the fluorescence decay of pyrene adsorbed on silica gel[29] and γ-alumina.[5]

The pyrene radical cation adsorbed on γ-alumina is formed following laser excitation at 337.1 nm, and electron transfer between ferrocene and the pyrene radical cation coadsorbed on γ-alumina[6] has been observed. The decay of the pyrene radical cation in the presence of ferrocene was fitted by Thomas et al.[6] using the dispersive kinetic model of Albery.[28] The observed rate constant from the Albery model $\bar{k}_{obs}$ was related to the total ferrocene concentration by the following equation:

$$\bar{k}_{obs} = \bar{k}_0 + k'_q\,[\text{quencher}]$$

where $\bar{k}_0$ is the average rate constant in the absence of quencher and k'_q is a bimolecular quenching rate constant. A linear correlation between the observed rate of pyrene radical cation decay and ferrocene concentration was observed in the range 0.2−1.08 μmol g^{-1}. The bimolecular rate constant (k'_q) for the quenching of the pyrene radical cation on γ-alumina ranged from 3.39 to 2.35×10^9 dm^2 mol^{-1} s^{-1} on increasing the temperature to which the silica was heated prior to adsorption from 130−350 °C.

In this paper we present results relating to the kinetics of electron transfer to the anthracene radical cation from coadsorbed electron donors on silica gel, and show that there is not a simple correlation between the free energy for electron transfer (ΔG_{et}) and the observed rate of electron transfer.

[⊗] Abstract published in *Advance ACS Abstracts,* June 1, 1997.

S1089-5647(97)00133-8 CCC: $14.00

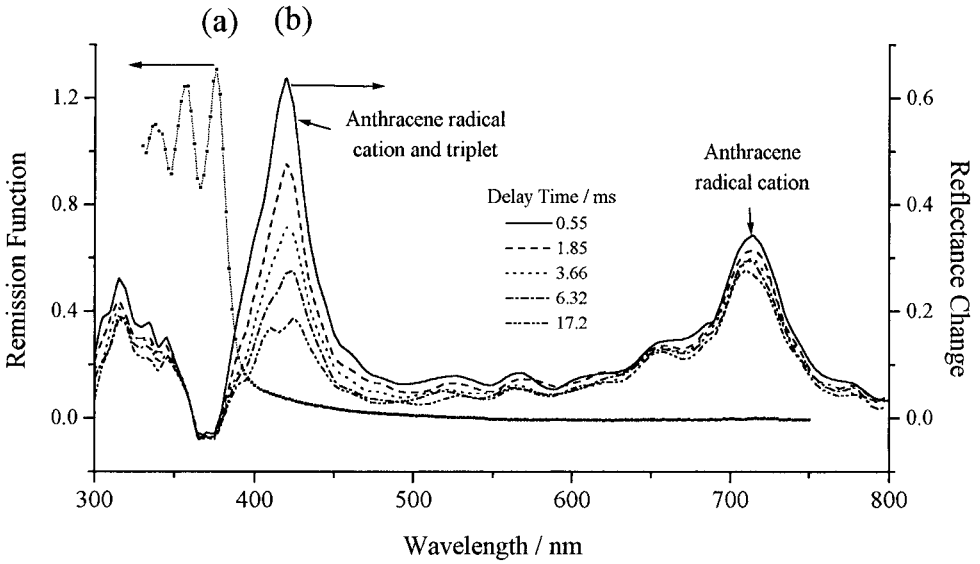

Figure 1. (a) Ground state diffuse reflectance absorption spectrum of anthracene adsorbed on silica gel at a sampling loading of 1.7 μmol g^{-1} shown as the Kubelka Munk remission function. (b) Time-resolved transient difference spectrum showing reflectance change $(R_0 - R_t)/R_0$ of the above sample following laser excitation at 355 nm. Laser pulse energy: 15 mJ cm^{-2}.

Experimental Section

Samples of anthracene on silica gel were prepared according to the method described in detail in ref 3. Briefly, silica gel (Davisil grade 635, Aldrich Chemical Company) was dried at 125 °C under vacuum to 5×10^{-5} mbar, and the vessel was repressurized with dry nitrogen. Anthracene (scintillation grade, Sigma) was dissolved in *n*-hexane or acetonitrile (spectrophotometric grade, Aldrich Chemical Company) previously dried by reflux over calcium hydride (Fisons), and the resulting solution was added to the dried silica gel. After equilibration for 3 h, the excess solution was decanted off and the sample dried under vacuum to 5×10^{-5} mbar. Sample loadings were in the range 0.56−40.9 μmol g^{-1}, as determined by analysis of the decanted solution. The incorporation of electron donors into the anthracene/silica gel system was achieved by the addition of *N*,*N*,*N*′,*N*′-tetramethyl-1,4-phenylenediamine (TMPD), azulene, triphenylamine (TPA), and *N*,*N*-dimethylaniline (DMA) to the anthracene solution prior to addition to the dried silica gel. Azulene was added from *n*-hexane; TMPD and DMA were added from acetonitrile; TPA was added from both *n*-hexane and acetonitrile.

Samples were also prepared by sublimation of anthracene and azulene onto silica gel. The procedure was as follows. The anthracene and azulene were dissolved in *n*-hexane and added to one arm of a two-armed vessel, and the *n*-hexane was removed under vacuum. The vessel was then repressurized, and the silica gel was added and then dried at 125 °C under vacuum to 5×10^{-5} mbar while the arm containing the azulene/anthracene mixture was placed in a Dewar of liquid nitrogen to prevent sublimation. The silica gel was taken from the heat, the vessel sealed, and the liquid nitrogen Dewar removed. The vessel was then left at room temperature under vacuum for 20 h with periodic agitation to allow sublimation of the anthracene and azulene onto the silica gel. The vessel was then evacuated to a pressure of 5×10^{-5} mbar, and the sample was then sealed into a cylindrical glass or quartz cuvette (22 mm diameter × 10 mm path length). Sample loadings were in the range 1.2−5.1 μmol g^{-1} azulene and approximately 0.5 μmol g^{-1} anthracene.

The sample geometry used in nanosecond diffuse reflectance laser flash photolysis has been described previously in detail in ref 30. Excitation of the samples was with the third harmonic of a HyperYAG Nd:YAG laser (Lumonics, 355 nm, 11 mJ per pulse). Diffusely reflected analyzed light from a 275 W xenon arc lamp (Oriel) was collected and focused onto the slit of an *f*/3.4 grating monochromator (Applied Photophysics) and detected with a side-on photomultiplier tube (Hamamatsu R928). Signal capture was either by a 2432A digital oscilloscope (Tektronix) or a Model 9845 transient digitizing card (EG&G), both interfaced to an IBM-compatible PC.

Millisecond diffuse reflectance flash photolysis studies were carried out using a Mecablitz 45 CL 1 photographic flashgun (Metz), with the UV filter removed, in place of the HY200 Nd:YAG laser, and its intensity was varied using neutral density filters. The rest of the flash photolysis apparatus was identical with that used in the nanosecond apparatus described above.

Ground state diffuse reflectance spectra and radical cation diffuse reflectance spectra at times greater than 20 s from the laser pulse were recorded on a PU8800 UV/VIS spectrophotometer (Phillips) equipped with an integrating sphere.

Results and Discussion

Anthracene on Silica Gel. As discussed in detail in a previous publication,[3] upon excitation at 355 nm of a sample of anthracene adsorbed onto silica gel the transient difference spectrum shows the presence of two species. The anthracene triplet state is characterized by triplet−triplet absorption peaking at 420 nm, while the radical cation is characterized by an absorption spectrum consisting of three peaks located at 715, 425, and 310 nm in approximately the ratio 2:1:1 (Figure 1). The assignment of these latter peaks as arising from the radical cation is on the basis of similarities with spectra seen in solution[31−34] and in zeolites.[20] Additionally, as discussed later, the decay of this spectrum in the presence of coadsorbed electron donors is accompanied by the concomitant appearance of the well-accepted spectrum of the cation radical of the electron donor,[33] as illustrated in Figure 5a for the TMPD−anthracene system. The production of the radical cation, in both the presence and absence of coadsorbed electron donors, has been proved to be multiphotonic by laser dose studies[3] and by millisecond flash photolysis studies, since upon millisecond flashlamp excitation a large triplet−triplet absorption is observed

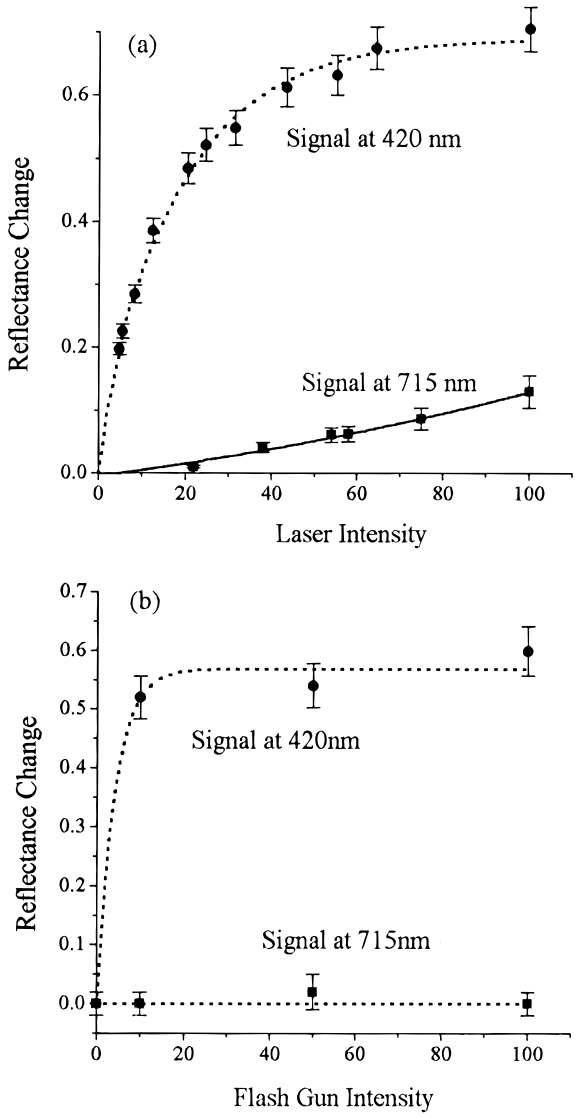

Figure 2. Change in reflectance $(R_0 - R_t)/R_0$ for the triplet (420 nm) and radical cation (715 nm) of anthracene adsorbed on silica gel at a loading of 3.4 μmol g^{-1} as a function of (a) laser intensity and (b) millisecond flashlamp intensity.

at 420 nm, comparable with that observed following laser excitation, but no radical cation absorption is seen at 715 nm. The shape of the plot of triplet−triplet absorption versus laser fluence provides an internal standard for a single-photon process produced by the laser, and the plot for the radical cation is completely different. This evidence, along with the fact that the ionization potential of anthracene, being 7.4eV,[26] is too high for single-photon ionization with 355 nm excitation confirms the multiphotonic production of the anthracene radical cation. Figure 2 shows the intensity of the anthracene radical cation (715 nm) and triplet−triplet (420 nm) absorptions as a function of laser fluence (Figure 2a) and flashgun intensity (Figure 2b) demonstrating the difference between the monophotonic triplet production and the multiphotonic nature of the radical cation production. The ejected electrons are either likely to be trapped in defect sites in the silica matrix, giving rise to so-called E′ centers absorbing in the ultraviolet,[35−39] or they might be expected to give rise to visible color centers as a result of hole trapping on impurities such as aluminum.[40] Such absorptions would overlap with the anthracene ground state and radical cation absorption spectra and this could explain why neither of these absorptions have been observed in these studies.

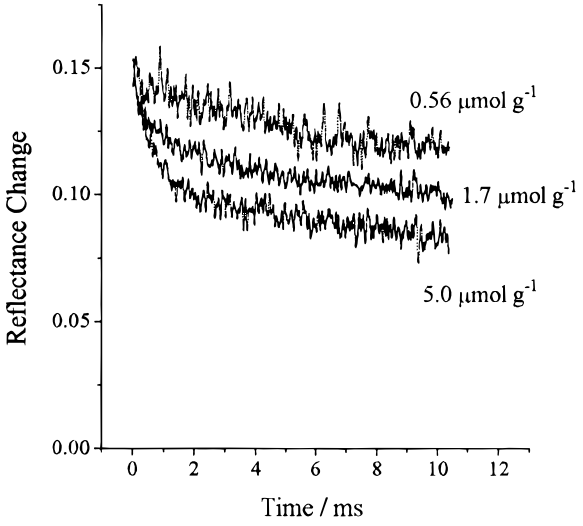

Figure 3. Anthracene radical cation decay kinetics following laser excitation at 355 nm, monitoring at 715 nm as a function of sample loading. Laser pulse energy: 15 mJ cm^{-2}.

Anthracene Radical Cation: Kinetic Analysis. The radical cation formed by laser excitation of anthracene adsorbed alone on silica gel remaining after the decay of the triplet state has a complex mechanism of decay occurring on time scales ranging from microseconds to hours. As the anthracene loading is increased from 0.56 to 40.9 μmol g^{-1}, the rate of the radical cation decay increases (Figure 3). Oelkrug et al.[7] have shown that the radical cations of distyrylbenzenes adsorbed on silica gel and alumina produced after laser excitation of low loadings (<0.7 μmol g^{-1}) decay via a mechanism based on geminate recombination, where the separation of electron and parent ion in the matrix is assumed small relative to the ion−ion separation distance. For this mechanism it can be shown[7] that the kinetics can be described by the expression

$$C_0/C = (1 + a\sqrt{t}) \quad (1)$$

where a is a constant and C and C_0 represent the concentration of the radical cation−electron pair at time $t = t$ and $t = 0$, respectively. Provided that there is an exponential falloff of transient concentration with sample depth and low reflectance changes (ΔR), C and C_0 can be replaced by ΔR and ΔR_0, respectively.[41,42]

Analysis of the decay kinetics of the anthracene radical cation using this expression reveals that at low loadings (<1.7 μmol g^{-1}) the decay of the radical cation is predominately by geminate recombination. This is shown by the linear plots obtained for $\Delta R_0/\Delta R$ versus $\sqrt{t}$ in Figure 4. At higher loadings the decay no longer conforms to this model, as would be expected since the sensitivity of the radical cation decay rate to the anthracene loading clearly shows that geminate recombination is not the dominant mechanism. Care was taken to ensure that even at high surface loadings ΔR was kept low in all experiments, and modeling studies have shown exponential falloffs of transient concentrations with sample depth for all loadings studied. Thus this change in kinetic mechanism can be rationalized since as sample loading increases, the ion−electron separation is no longer small relative to the ion−ion separation distance and bulk diffusion of electrons is likely to compete efficiently with geminate recombination.

Anthracene Radical Cation Decay in the Presence of Electron Donors. The addition of an electron donor to the system causes an increase in the rate of radical cation decay,

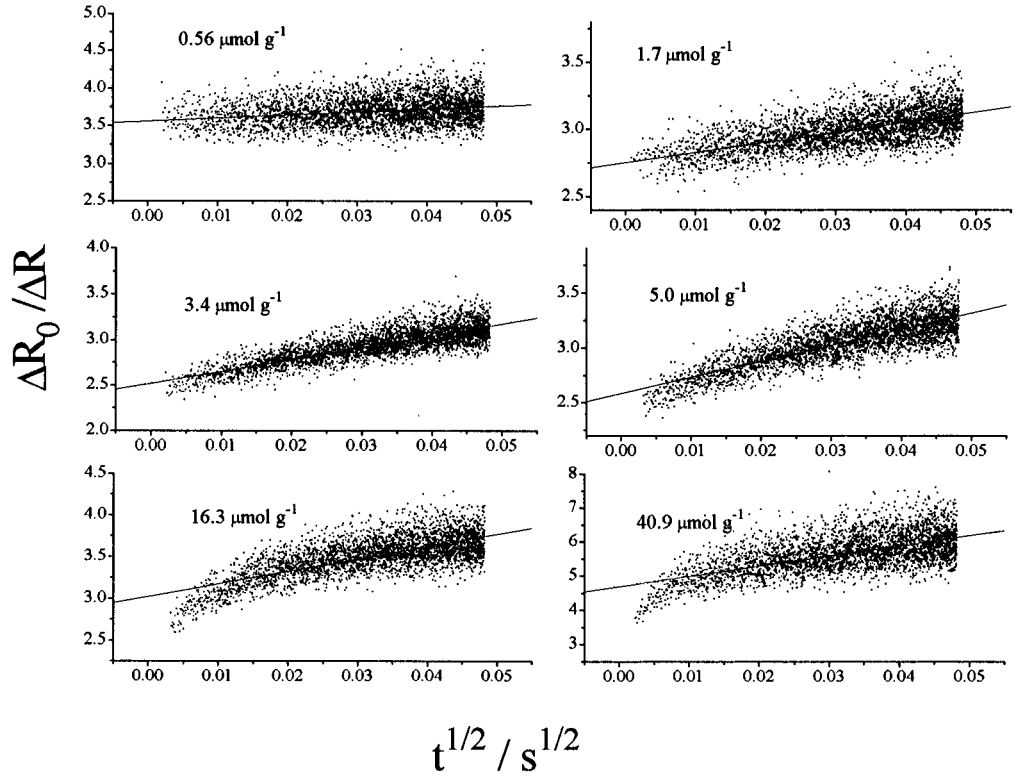

Figure 4. Initial anthracene radical cation decay (plotted as $\Delta R_0/\Delta R$) versus $\sqrt{t}$ as a function of anthracene loading.

provided that the oxidation potential of the donor does not exceed 1.09 V (vs SCE), which is the reduction potential of the anthracene radical cation.[43] In the cases of TMPD, TPA, and DMA, this accelerated radical cation decay is accompanied by the concomitant appearance of the cation radical of the electron donor (Figure 5a−c). The formation of the azulene radical cation is not clearly observed (Figure 5d) when azulene is used as an electron donor. This is due to the location and intensity of the azulene radical cation absorption peaks, the principle one of which is located at 368 nm, underneath the anthracene ground state absorption. Other peaks at 480 and 830 nm are of much lower intensity, and indeed 830 nm is outside our analyzing range. In all cases kinetic analysis of the electron transfer process is performed by monitoring the decay of the anthracene radical cation absorption at 715 nm. In the case of TPA as electron donor the absorption remaining at long times at 715 nm assigned as due to the TPA radical cation is allowed for in the analysis. This can readily be done since the TPA radical cation decays on a considerably longer time scale than the anthracene radical cation under these conditions. In the presence of electron donors the rate of decay of the radical cation is considerably faster than in their absence, and hence the assumption can validly be made that all of the observed decay is due to electron transfer from the electron donor to the radical cation of anthracene.

The decay kinetics of the anthracene radical cation in the presence of electron donors are again complex and do not conform to a single exponential model. Two models which have been shown to successfully describe kinetics in heterogeneous media[1−3,5,6,21,23,28,29,44−49] have been applied to this data. These are a dispersive kinetic model[28] assuming a distribution of rate constants for the observed reaction, and a model assuming a bimolecular reaction taking place on a fractal dimensional surface which has been applied successfully to triplet−triplet annihilation reactions.[1−3]

Dispersive Kinetic Model.[28] This model assumes a Gaussian distribution of activation energies for the kinetic decay process, corresponding to a logarithmic Gaussian distribution of rate constants. The data is fitted with the equation

$$\frac{C}{C_0} = \frac{\int_{-\infty}^{+\infty} \exp(-t^2)\exp[-\bar{k}t\exp(\gamma t)]\,dt}{\int_{-\infty}^{+\infty}\exp(-t^2)\,dt} \qquad (2)$$

transformed according to the appendix in ref 28 to give finite integrals. Here C_0 and C are the concentrations of transient at time $t = 0$ and $t = t$, respectively, γ is the distribution width, and $\bar{k}$ is the mean rate constant. Provided that the reflectance change is small, ΔR can be substituted for C. According to this analysis a plot of reflectance change versus ln(time) should give a smooth sigmoid curve. This is found for all the electron donors employed. As can clearly be seen from Figure 6, where reflectance change versus ln(time) is plotted for a range of TMPD concentrations, the value of the mean decay rate constant increases with increasing electron donor loading, while the width of the distribution remains approximately constant. A linear dependence of the mean rate constant for anthracene radical cation disappearance with electron donor loading is obtained for the concentration range employed for TMPD, TPA, DMA, and azulene (shown for TMPD and azulene in Figure 7a); thus in the presence of coadsorbed electron donors of concentration [ED], the rate of electron transfer ($\bar{k}_{et}$) from the electron donor to the anthracene radical cation can be determined by

$$\bar{k}_{obs} = \bar{k}_0 + \bar{k}_{et}[\mathrm{ED}]$$

where $\bar{k}_0$, the intercept of these plots, is zero to within experimental error. This near-zero intercept demonstrates the validity of the assumption that electron transfer is the dominant deactivation mechanism in the presence of electron donors.

Fractal Dimensional Model[1,2] *Used for the Analysis of the Anthracene Radical Cation Decay Curves in the Presence of TMPD and Azulene.* A kinetic scheme has previously been used by us[3] and others[1,2] to describe the decay of delayed fluorescence

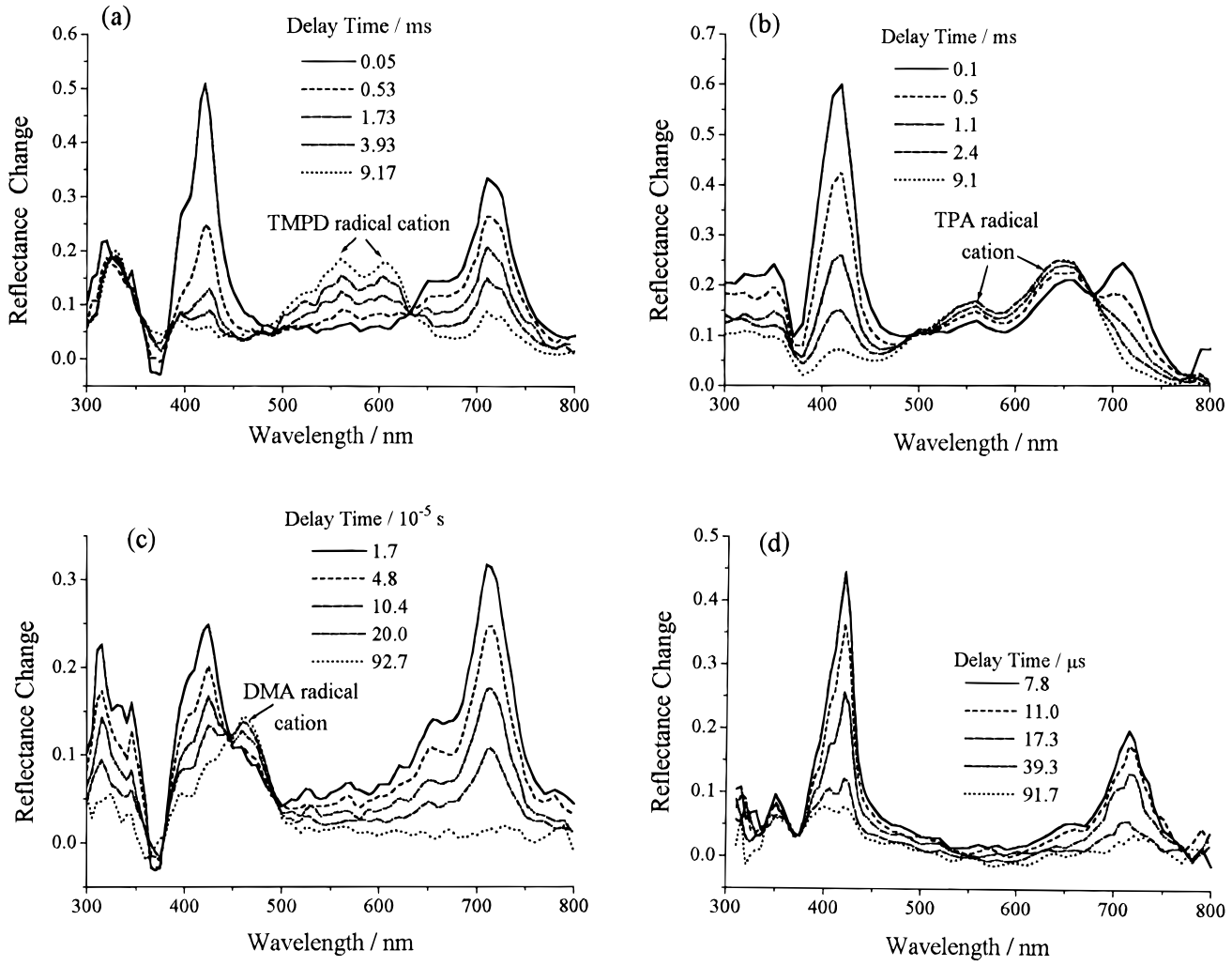

Figure 5. Time-resolved transient difference spectra showing reflectance change $(R_0 - R_t)/R_0$ following laser excitation at 355 nm of (a) anthracene and *N,N,N′,N′*-tetramethyl-1,4-phenylenediamine adsorbed on silica gel at loadings of 0.7 and 1.7 μmol g^{-1} respectively, (b) anthracene and triphenylamine adsorbed on silica gel at loadings of 2 and 0.4 μmol g^{-1} respectively, (c) anthracene and *N,N*-dimethylaniline adsorbed on silica gel at loadings of 2 and 0.7 μmol g^{-1} respectively, and (d) anthracene and azulene adsorbed on silica gel at loadings of 2 and 1.6 μmol g^{-1} respectively. Laser pulse energy: 15 mJ cm^{-2}.

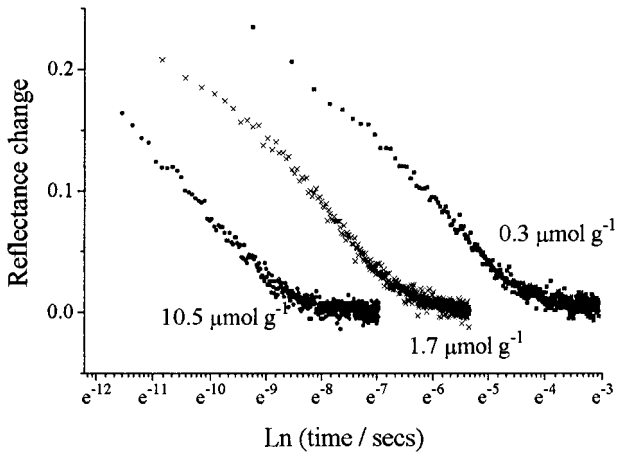

Figure 6. Kinetic decay at 715 nm of the anthracene radical cation coadsorbed with TMPD, following laser excitation at 355 nm, as a function of TMPD loading.

arising from triplet−triplet annihilation on silica gel. Since this model concerns bimolecular reactions on heterogeneous surfaces, it has been applied to a selection of the data to see how well it fits. The model involves the use of a fractal dimensional rate constant, and its derivation assumes the following scheme for the anthracene radical cation ($An^{\bullet+}$) decay:

$$An^{\bullet+} + ED \rightarrow An + ED^{\bullet+}$$

If a fractal dimensional model is assumed, we can define an instantaneous rate coefficient k_2, where $k_2 = k_2^0 t^{-h}$ and $h = 1 - (d_s/2)$, where d_s is the spectral dimension. In the percolation limit, the spectral dimension $d_s = 4/3$[50,51] so $h = 1/3$ and

$$\left(\ln \frac{\Delta R^0}{\Delta R}\right)^{3/2} = \left(\frac{3}{2} k_2^0 [ED]_0\right)^{3/2} t \qquad (3)$$

where again ΔR can be used interchangeably with concentration provided ΔR is small.

For a two-dimensional model, $h = 0$ at early times[52] and

$$\ln \frac{\Delta R^0}{\Delta R} = k_2 t [ED]_0 \qquad (4)$$

If the fractal or two-dimensional model holds, a plot $(\ln(\Delta R^0/\Delta R))^\eta$ versus t will yield a straight line for either $\eta = 1$ (two-dimensional model) or $\eta = 3/2$ (fractal dimensional model). The gradient of these graphs will be equal to $k_2[ED]_0$ for the two-dimensional model and $((3/2)k_2^0[ED]_0)^{3/2}$ for the fractal model. Hence k_2 for the two-dimensional model and k_2^0 for the

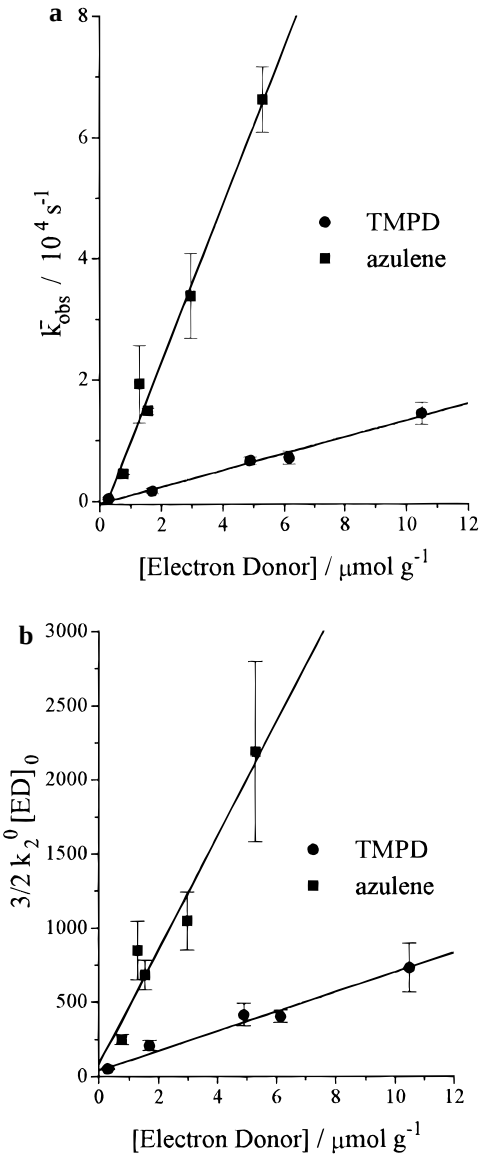

Figure 7. Average rate constant for electron transfer from both TMPD and azulene to the anthracene radical cation, formed following laser excitation at 355 nm, shown using (a) $\bar{k}_{obs}$ from the dispersive kinetic model and (b) $(3/2)k_2^0[ED]_0$ from the fractal model, plotted versus electron donor concentration.

fractal model can be calculated from the gradient and a knowledge of the electron donor concentration. Transient decay data for the anthracene radical cation coadsorbed with both TMPD and azulene have been analyzed using these models. The analysis based on the fractal dimensional decay mechanism fits the electron transfer data well at early times (Figure 8a). A similar analysis based on the two-dimensional decay model does not yield good fits to the data (Figure 8b). Again, as in the dispersive kinetic analysis, a linear correlation between the fractal dimensional rate constant for electron transfer k_2^0 and electron donor loading is observed following analysis of the data at early times in the decay with this model for both TMPD and azulene (Figure 7b) coadsorbed with anthracene.

Hence both the dispersive kinetic model and the fractal dimensional model can adequately describe the data. However the dispersive kinetic model fits the kinetic decay at all times, while the fractal dimensional model only describes the initial part of the decay, as expected owing to the assumptions in the derivation of the model. The decay is expected to become more two-dimensional at longer times;[1−3] hence the fractal dimensional model only applies to early times. Also the units of k_2^0 are equal to g mol^{-1} $s^{-2/3}$, which makes the values difficult to compare with rate constants observed by others.

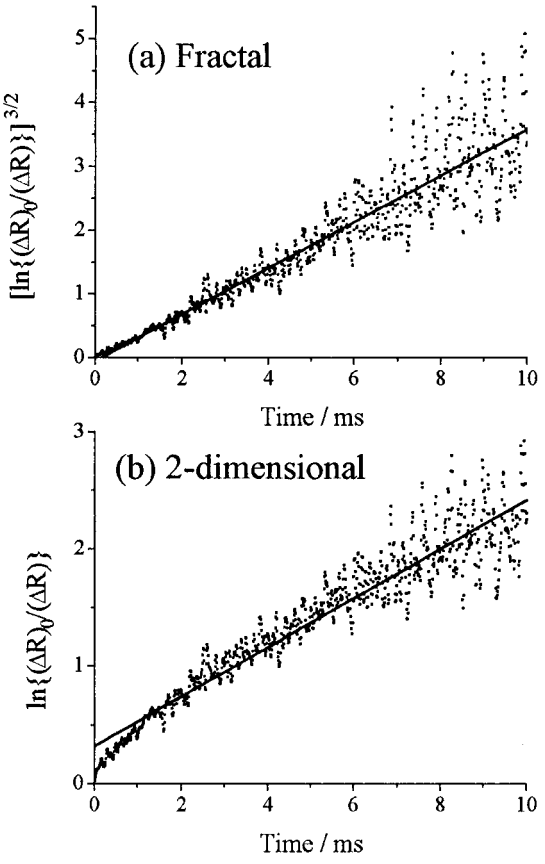

Figure 8. Kinetic decay traces of the anthracene radical cation coadsorbed with TMPD fitted using (a) the fractal dimensional model and (b) the two-dimensional model.

Summary of the Electron Transfer Data

A linear correlation between decay rates and electron donor concentration was observed for TMPD, azulene, TPA, and DMA. The gradients of plots of observed rate constant for anthracene radical cation decay versus electron donor are summarized in Table 1, as a function of the oxidation potential of the electron donor and the free energy of electron transfer (ΔG_{et}).

Table 1 summarizes the results obtained with the different kinetic models and electron donors. The fact that azulene sublimed onto silica gel and adsorbed from solution gives the same rate for electron transfer implies that these rates are actual surface properties and are not solvent mediated. TPA adsorbed from hexane or acetonitrile shows rate constants for electron transfer which overlap for the 95% confidence limits, again suggesting solvent mediation does not play a significant role. In addition, the absolute rates of electron transfer do not show a simple correlation with the electron donor oxidation potentials; this is most clearly illustrated on comparing k_{et} for azulene and TMPD.

It is well established that the rate of electron transfer in solution is composed of two components; the rate of diffusion of the molecules so as to become nearest neighbours and the rate of electron transfer in the encounter pair. Debye[53] showed that by assuming the radius for reaction is equal to the sum of the radii of the reacting moieties, and that the rate of reaction is equal to the rate of their diffusion, then the rate of diffusion-controlled reaction of molecules in solution is independent of

TABLE 1: Electron Donor Oxidation Potentials,[43] Free Energy for Electron Transfer, and Rate Constants for Electron Transfer, between Electron Donors and Anthracene Radical Cation[a]

electron donor[b]	oxidation potential/V (vs SCE)	ΔG_{et}/eV	$\bar{k}_{et}$/g mol^{-1} s^{-1}	k_2^0/g mol^{-1} s$^{-2/3}$
TMPD (ACN)	0.32	−0.77	$(1.4 \pm 0.8) \times 10^9$	$(6.3 \pm 0.6) \times 10^7$
DMA (ACN)	0.53	−0.56	$(1.5 \pm 0.2) \times 10^{10}$	
azulene (ACN)	0.71	−0.38	$(1.3 \pm 0.1) \times 10^{10}$	$(3.8 \pm 0.5) \times 10^8$
azulene (sublimed)			$(1.3 \pm 0.4) \times 10^{10}$	
TPA (ACN)	0.92	−0.17	$(4.6 \pm 0.8) \times 10^8$	
TPA (HEX)			$(2.7 \pm 0.9) \times 10^8$	
naphthalene (HEX)	1.54	0.45	no electron transfer	

[a] Errors quoted are one standard deviation. [b] ACN, acetonitrile; HEX, *n*-hexane.

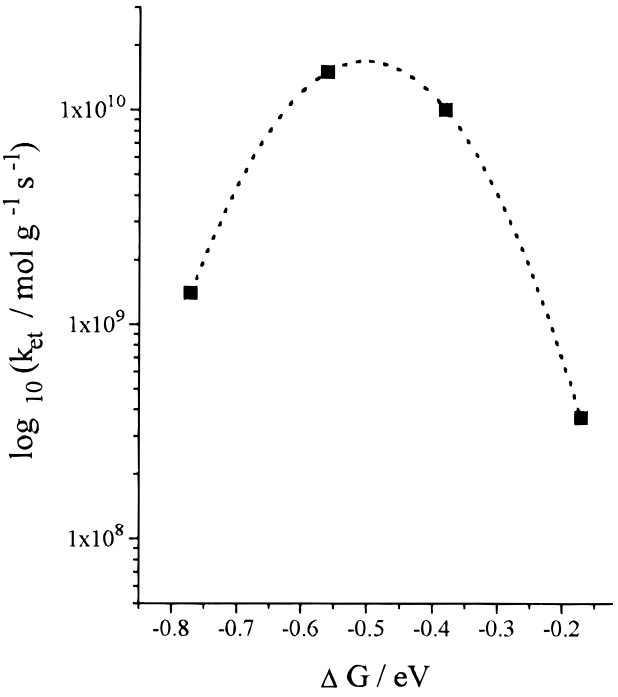

Figure 9. Rate of electron transfer from various electron donors to the anthracene radical cation, formed following laser excitation at 355 nm, plotted as $\log_{10} k_{et}$ versus ΔG_{et} in eV.

the identity of those molecules. The rate of electron transfer on surfaces would also be expected to be governed by the rate of diffusion on the surface and the rate of electron transfer in the encounter pair. On silica gel the rates of diffusion of different molecules cannot be assumed to be equal due to differing strengths of adsorption to the surface; hence if the rate-limiting step is surface diffusion then the rate will not be independent of the identities of the diffusing moieties. If this is the case, anthracene radical cation decay in the presence of an electron donor on silica gel will not be exclusively governed by the value of ΔG_{et}.

Marcus theory suggests that the rate of electron transfer, while increasing with ΔG_{et} at low ΔG_{et} values should actually show an inverse correlation with ΔG_{et} at higher values.[54,55] A plot of the logarithm of the rate of electron transfer versus ΔG_{et} for electron transfer reveals an apparent Marcus type inverted region (Figure 9). This behavior is surprising with such low $-\Delta G_{et}$ values when compared with those obtained in solution,[56] although as yet no other studies of this nature have been carried out on silica gel. However, in solution the absence of an inverted region at these $-\Delta G_{et}$ values may be due to diffusion taking over as the rate-controlling mechanism; Thomas et al.[56] found that k_{et} was independent of ΔG_{et} in this region in methanol solution, suggesting a diffusion-controlled reaction. The presence of this apparent Marcus inverted region shown in Figure 9 cannot be confirmed with so few samples, and considering the structural differences in the electron donors and their consequent differing heats of adsorption, the rate-limiting step is considered most likely to be diffusion of the electron donor molecules to the anthracene radical cation, with the rate of electron transfer within the encounter pair being relatively fast. A related explanation is that there is a distribution of sites of differing accessibility which inflict steric restrictions on the encounter pair, making the observed rates depend on the ease with which the anthracene and electron donor can interact in a favorable orientation.

The variation in k_{et} observed for the electron donors studied requires further experiments in order to distinguish between the proposed mechanisms. For this system such distinction should be possible since all of the observed transients have been unambiguously assigned, and we have shown that the observed electron transfer rate can be well described using a dispersive kinetic model. Of the other studies detailed in the literature involving electron transfer on silica gel, very few present a detailed kinetic analysis and hence there is little data with which to compare our values. However, rates of electron transfer from the methylviologen monopositive radical cation to polychloroalkanes determined by Thomas et al.[47] are of a similar magnitude to ours, although with so few results this does little to resolve the question of mechanism.

Summary

The production of the anthracene radical cation is multiphotonic in nature. If no electron donor is present in the anthracene/silica gel system, then electron−radical combination is the dominant decay mechanism. At low loadings geminate recombination occurs; for more concentrated samples electrons combine with radicals other than their parent as the ion−ion separation approaches the ion−electron separation. Electron transfer to the anthracene radical cation can be achieved using coadsorbed electron donors, regenerating anthracene and generating the electron donor radical cation, provided that the oxidation potential of the electron donor is greater than the reduction potential of the anthracene radical cation. This rate of electron transfer, as described with the dispersive kinetic model of Albery et al., is seen to increase linearly as a function of electron donor surface loading, allowing rate constants for the electron transfer to be evaluated. We have established that the rate constants for the electron transfer do not show a linear correlation with the oxidation potential of the donor, as would be expected if the electron transfer step itself were rate determining. However, this lack of a simple correlation may be explained by the presence of a Marcus inverted region, and further experiments are being carried out to see if this Marcus type dependence applies to other systems. The lack of a linear correlation of the electron transfer rate constants on ΔG_{et} can also be explained on the basis of surface diffusion being rate determining. That azulene would have a greater diffusion rate on silica than TMPD is not unexpected, since TMPD will be

held to the surface through hydrogen bonding with the terminal nitrogens, while azulene will interact with the surface through π-cloud interactions and the heat of adsorption through hydrogen bonding is known to be greater than that for π-cloud interactions.[57]

Acknowledgment. We thank the Engineering and Physical Sciences Research Council for financial support.

References and Notes

(1) Oelkrug, D.; Uhl, S.; Wilkinson, F.; Willsher, C. J. *J. Phys. Chem.* **1989**, *93*, 4551.
(2) Oelkrug, D.; Gregor, M.; Reich, S. J. *Photochem. Photobiol.* **1991**, *54*, 539.
(3) Wilkinson, F.; Worrall, D. R.; Williams, S. L. *J. Phys. Chem.* **1995**, *99*, 6689.
(4) Bauer, R. K.; de Mayo, P.; Natarajan, L. V.; Ware, W. R. *Can. J. Chem.* **1984**, *62*, 1279.
(5) Pankasem, S.; Thomas, J. K. *J. Phys. Chem.* **1991**, *95*, 7385.
(6) Pankasem, S.; Thomas, J. K. *J. Phys. Chem.* **1991**, *95*, 6990.
(7) Olekrug, D.; Reich, S.; Wilkinson, F.; Leicester, P. A. *J. Phys. Chem.* **1991**, *95*, 269.
(8) Kelly, G.; Willsher, C. J.; Wilkinson, F.; Netto-Ferreira, J. C.; Olea, A.; Weir, D.; Johnston, L. J.; Scaiano, J. C. *Can. J. Chem.* **1990**, *68*, 812.
(9) Frederick, B.; Johnston, L. J.; de Mayo, P.; Wong, S. K. *Can. J. Chem.* **1984**, *62*, 403.
(10) Lednev, I. K.; Mathivanan, N.; Johnston, L. J. *J. Phys. Chem.* **1994**, *98*, 11444.
(11) Beck, G.; Thomas, J. K. *Chem. Phys. Lett.* **1983**, *94*, 553.
(12) Oelkrug, D.; Krabichler, G.; Honnen, W.; Wilkinson, F.; Willsher, C. J. *J. Phys. Chem.* **1988**, *92*, 3589.
(13) Mao, Y.; Thomas, J. K. *Langmuir* **1992**, *8*, 2501.
(14) Mao, Y.; Thomas, J. K. *J. Chem. Soc., Faraday Trans.* **1992**, *88*, 3079.
(15) Iu, K-K.; Thomas, J. K. *Langmuir* **1990**, *6*, 471.
(16) Johnston, L. J.; Scaiano, J. C.; Shi, J-L.; Siebrand, W.; Zerbetto, F. *J. Phys. Chem.* **1991**, *95*, 10018.
(17) Ramamurthy, V.; Sanderson, D. R.; Eaton, D. F. *J. Phys. Chem.* **1993**, *97*, 13380.
(18) Park, J.; Kang, W-K.; Ryoo, R.; Jung, K-H.; Jang, D-J. J. *Photochem. Photobiol. A: Chem.* **1994**, *80*, 333.
(19) Hashimoto, S.; Fukazawa, N.; Fukumura, H.; Masuhara, H. *Chem. Phys. Lett.* **1994**, *219*, 445.
(20) Iu, K. K.; Thomas, J. K. *J. Phys. Chem.* **1991**, *95*, 506.
(21) Liu, X.; Thomas, J. K. *Langmuir* **1993**, *9*, 727.
(22) Liu, X.; Iu, K-K.; Thomas, J. K. *Chem. Phys. Lett.* **1993**, *204*, 163.
(23) Iu, K-K.; Liu, X.; Thomas, J. K. *J. Phys. Chem.* **1993**, *97*, 8165.
(24) Iu, K-K.; Liu, X.; Thomas, J. K. *J. Photochem. Photobiol. A: Chem.* **1994**, *79*, 103.
(25) Liu, X.; Iu, K-K.; Thomas, J. K.; He, H.; Klinowski, J. *J. Am. Chem. Soc.* **1994**, *116*, 11811.
(26) Murov, S. L.; Carmichael, I.; Hug, G. L. *Handbook of Photochemistry*, 2nd ed.; Marcel Dekker: New York, 1993; Table 10a-3. Data taken from: Levin, R. D.; Lias, S. G. NSRDS-NBS **1982**, *71*, 634 (National Bureau of Standards: Washington, DC). Lias, S. G.; Bartmess, J. E.; Liebman, J. F.; Holmes, J. L.; Levin, R. D.; Mallard, W. G. *J. Phys. Chem. Ref. Data* **1988**, *17*, 861. Lias, S. G.; Bartmess, J. E.; Liebman, J. F.; Holmes, J. L.; Levin, R. D.; Mallard, W. G. *NIST Positive Ion Energetics Database: Version 1.1*; National Institute of Standards and Technology: Gaitherburg, MD, 1990.
(27) Wilkinson, F.; Beer, R. *Photochemical Processes in Organised Molecular Systems*; Honda, K., Ed.; Elsevier Science: Amsterdam, 1991; pp 377−396.
(28) Albery, W. J.; Bartlett, P. N.; Wilde, C. P.; Darwent, J. R. *J. Am. Chem. Soc.* **1985**, *107*, 1854.
(29) Krasnansky, R.; Koike, K.; Thomas, J. K. *J. Phys. Chem.* **1990**, *94*, 4521.
(30) Kessler, R. W.; Wilkinson, F. *J. Chem. Soc., Faraday Trans.* 1, **1981**, *77*, 309.
(31) Wang, Z.; Weininger, S. J.; McGimpsey, W. G. *J. Phys. Chem.* **1993**, *97*, 374.
(32) Shida, T.; Iwata, S. *J. Am. Chem. Soc.* **1973**, *95*, 3473.
(33) Shida, T. *Physical Sciences Data 34, Electronic Absorption Spectra of Radical Ions*; Elsevier Science: Amsterdam, 1988.
(34) Liu, A.; Sauer, M. C.; Loffredo, D. M.; Trifunac, A. D. *J. Photochem. Photobiol. A: Chem.* **1992**, *647*, 197.
(35) Nelson, C. M.; Weeks, R. A. *J. Appl. Phys.* **1961**, *32*, 883.
(36) Weeks, R. A.; Fell, E. J. *J. Appl. Phys.* **1964**, *35*, 1932.
(37) Compton, W. D.; Arnold, G. W. *Discuss. Faraday Soc.* **1961**, *31*, 130.
(38) Arnold, G. W.; Compton, W. D. *Phys. Rev.* **1959**, *116*, 802.
(39) Levy, P. W. *J. Phys. Chem. Solids* **1960**, *13*, 287.
(40) Thomas, J. K. *Chem. Rev.* **1993**, *93*, 301.
(41) Lin, T.-P.; Kan, H. K. A. *J. Opt. Soc. Am.* **1970**, *60*, 1252.
(42) Kessler, R. W.; Krabichler, G.; Uhl, S.; Oelkrug, D.; Hagan, W. P.; Hyslop, J.; Wilkinson, F. *Opt. Acta* **1983**, *30*, 1099.
(43) Murov, S. L.; Carmichael, I.; Hug, G. L. *Handbook of Photochemistry*, 2nd ed.; Marcel Dekker: New York, 1993; Tables 10b-1 and 10b-2. Data taken from: Siegerman, H. *Technique of Electroorganic Synthesis*; Techniques of Chemistry, Vol. 5, Part II; Weinberg, N. L., Ed.; John Wiley: New York, 1975; pp 667−1056. Zweig, A.; Lancaster, J. E.; Neglia, M. T.; Jura, W. H. *J. Am. Chem. Soc.* **1964**, *86*, 4130. Pysh, E. S.; Yang, N. C. *J. Am. Chem. Soc.* **1963**, *85*, 2124.
(44) Levin, P. P.; Katalnikov, I. V.; Ferreira, L. F. V.; Costa, S. M. B. *Chem. Phys. Lett.* **1992**, *193*, 461.
(45) Levin, P. P.; Costa, S. M. B.; Ferreira, L. F. V. *J. Photochem. Photobiol. A: Chem.* **1994**, *82*, 137.
(46) Liu, X.; Mao, Y.; Reutten, S. A.; Thomas, J. K. *Sol. Energy Mater. Sol. Cells* **1995**, *38*, 199.
(47) Mao, Y.; Breen, N. E.; Thomas, J. K. *J. Phys. Chem.* **1995**, *99*, 9909.
(48) Levin, P. P.; Costa, S. M. B.; Ferreira, L. F. V. *J. Phys. Chem.* **1995**, *99*, 1267.
(49) Hite, P.; Krasnansky, R.; Thomas, J. K. *J. Phys. Chem.* **1986**, *90*, 5795.
(50) Alexander, S.; Orbach, R. *J. Phys. Lett.* **1982**, *43*, 625.
(51) Leyfraz, F.; Stanley, H. E. *Phys. Rev. Lett.* **1983**, *51*, 2048.
(52) Kopelman, R. In *The Fractal Approach to Heterogeneous Chemistry*; Avnir, D., Ed.; John Wiley and Sons: New York, 1989; pp 296−299.
(53) Debye, P. J. *Trans. Electrochem. Soc.* **1942**, *82*, 265.
(54) Marcus, R. A. *J. Chem. Phys.* **1956**, *24*, 966.
(55) Marcus, R. A. *Annu. Rev. Phys. Chem.* **1964**, *15*, 155.
(56) Koike, K.; Thomas, J. K. *J. Chem. Soc., Faraday Trans.* **1992**, *88*, 195.
(57) Yakimova, O. I.; Eremenko, A. M.; Chuiko, A. A. *J. Mol. Struct.* **1990**, *218*, 447.